Retrieval and characterization of carbon monoxide (CO) vertical profiles in the Martian atmosphere from observations of PFS/MEX

Jimmy Bouche[a], Sophie Bauduin[a], Marco Giuranna[b], Séverine Robert[c], Shohei Aoki[c,d,e], Ann Carine Vandaele[c], Justin T. Erwin[c], Frank Daerden[c], Paulina Wolkenberg[b,f], Pierre-François Coheur[a]

[a] *Université libre de Bruxelles (ULB), Atmospheric spectroscopy, Service de Chimie Quantique et Photophysique CP 160/09, Avenue F.D. Roosevelt 50, Bruxelles, Belgium.*
[b] *National Institute of Astrophysics INAF-IAPS, Rome, Italy.*
[c] *Royal Belgian Institute for Space Aeronomy, Brussels, Belgium.*
[d] *Fonds National de la Recherche Scientifique, Belgium.*
[e] *Tohoku University, Japan.*
[f] *Space Research Centre of Polish Academy of Sciences, Warsaw, Poland.*

Abstract

The knowledge of the carbon monoxide (CO) abundance on Mars is essential in order to assess the processes driving the carbon cycle on the planet. Solar occultation measurements provide vertically-resolved measurements of CO from a few kilometers to higher altitudes and can be complemented by nadir measurements to enhance the spatial coverage of observations and the monitoring of the near-surface layer. Up to now, CO retrievals from nadir observations have, however, mostly been performed on mean spectra in the shortwave and only total column abundances have been obtained. In this work we explore the possibility of exploiting nadir measurements from the Planetary Fourier Spectrometer (PFS) in the 1–0 band of CO to retrieve vertical profiles of that species on individual pixels (single measurement). The retrievals are performed for a set of 16 representative PFS spectra with reasonable signal-to-noise ratios by applying the optimal estimation method with appropriate constrains, built from model simulations of the Martian atmosphere. The retrieved profiles are characterized in terms of vertical sensitivity and errors. We demonstrate in particular that the PFS nadir measurements carry information mostly on the CO column below 15 km, with a maximum sensitivity to the surface atmosphere. These measurements allow

to substantially reduce the prior uncertainty on the CO abundance in this altitude range, with an estimated total retrieval error on the column-averaged volume mixing ratio around 10%. We show that the set of retrieved VMRs agree reasonably with measurements from other instruments considering the different time periods investigated. The retrieved VMRs also capture well the known spatial and seasonal CO variability, which is promising in the perspective of exploiting more largely the exceptional set of PFS observations on Mars.

Keywords:
PFS, Mars Express, carbon monoxide, vertical sensitivity, seasonal variability

---

1. Introduction

The first detection of carbon monoxide (CO) in the atmosphere of Mars has been made 50 years ago by [1] using ground-based observations. Since then, it has been discovered that CO plays a major role in the carbon photochemical cycle. CO is indeed formed by the photolysis of carbon dioxide (CO_2) and its recombination with oxygen (O) atoms is at the center of the so-called stability problem of CO_2 in the Martian atmosphere. This reaction is spin-forbidden and extremely slow compared to the recombination of O atoms into O_2. As a consequence, without an efficient recycling process, the total amount of CO_2 would have been converted into its photolysis products, and the abundance of CO and O_2 in the Martian atmosphere would have significantly exceeded the present amount. In reality, as proposed in the 1970's by [2] and [3], the recombination of CO into CO_2 is catalysed by odd hydrogen (H, OH and HO_2 and generally written HO_x) formed by the photodissociation of water vapour (H_2O). These earlier models were, however, not completely satisfactory; they used either an eddy diffusion coefficient unacceptably large for the middle atmosphere of Mars [2] or an amount of H_2O significantly exceeding the known values [3]. Although more recent models have solved some of these shortcomings [4, 5, 6, 7, 8], the global carbon cycle on Mars is nowadays still not completely understood. The contribution of heterogeneous chemistry [9, 10] in the different processes at play is part of the remaining uncertainties. The recently reported but debated detection of atmospheric methane, combined with its large apparent seasonal variability, has challenged further the understanding of the carbon cycle. To improve on

this understanding, more and more accurate observations of the spatial, vertical and temporal variability of the different species involved in the carbon cycle on Mars are obviously needed.

This has already been partly the case for CO, for which the knowledge of spatial and seasonal variations in the Martian atmosphere has improved thanks to different remote observations, made from ground or from satellites in the last 15 years. Contrary to what has been considered for a long time, it was shown that CO was not uniformly mixed but has strong latitudinal and seasonal variations, intimately related to the condensation-sublimation cycle of CO_2 at the poles. The first evidence of the variability comes from ground-based observations by [11], who reported a north-to-south increase of the CO volume mixing ratio (VMR) during the Northern summer due to the condensation of CO_2 at the south polar cap. Since then, a more complete picture of the latitudinal-seasonal changes of CO has been brought thanks to different instruments, such as OMEGA (Observatoire pour la Minéralogie, l'Eau, les Glaces et l'Activité) [12] and PFS (Planetary Fourier Spectrometer) [13, 14, 15] on-board Mars Express (MEX), and CRISM (Compact Reconnaissance Imaging Spectrometer for Mars) [16, 17] on-board the Mars Reconnaissance Orbiter (MRO). However, there has been no systematic retrieval of the CO vertical profile, especially from nadir observations. The only study of this kind has attempted to exploit different spectral ranges or instruments to retrieve information on the CO vertical distribution [18], but these synergetic approaches are difficult to implement. This is in stark contrast to Earth, where the retrieval of vertical profile is becoming standard. For CO in particular, it has been shown for thermal infrared (TIR) sounders that, in case of high temperature contrasts between the ground and the air above it (hereafter called thermal contrast), two partial columns of CO can be decorrelated for the lower part of the atmosphere (surface layer and rest of the troposphere) [19]. If possible on Mars, the retrieval of CO profiles, even if weakly resolved, would provide useful constraints for the models regarding the carbon chemistry in the atmosphere close to the surface, a region generally not accessible to limb/solar occultation measurements. This work examines therefore the possibility of retrieving information on the CO vertical distribution from Martian nadir TIR observations. This is performed on a small set of single PFS nadir spectra, chosen to represent different conditions of CO on Mars, in the region of the CO fundamental vibrational band ($\sim$ 2150 cm^{-1}). The optimal estimation method [20] is used, which allows for a detailed characterization of the retrieved CO profiles in terms of error budget

and vertical sensitivity. Section 2 presents the PFS instrument and section 3 is dedicated to a short description of the radiative transfer. Section 4 introduces the optimal estimation method. The selection of PFS observations and the retrieval settings are described in section 5 and the results are discussed in section 6, with a detailed interpretation of the error budget of the CO retrieved. The conclusions of the study are summarized in section 7.

2. PFS instrument

PFS [21] is a double pendulum Fourier transform interferometer on-board the Mars Express spacecraft. It circles Mars on a quasi-polar orbit with an inclination of 87° and a pericentre altitude of around 250 km. It covers a large spectral range in the infrared (250-8200 cm^{-1}) thanks to two different channels: the Long Wavelength Channel (LWC, 250–1700 cm^{-1}) and the Short Wavelength Channel (SWC, 1700–8200 cm^{-1}). PFS records Martian atmospheric spectra at a spectral resolution of 1.3 cm^{-1} before apodization for both channels and has a spectral sampling of (around) 1 cm^{-1}. The instrument has a field-of-view (IFOV) of about 1.6° (full width at half maximum, FWHM) for the SWC and of 2.8° (FWHM) for the LWC, which corresponds to a spatial resolution on ground of 7 and 12 km respectively, when PFS is at 250 km from Mars. A full description of the PFS design, specification and operation can be found in [21]. Additional details about the spectral and radiometric calibration procedure for both channels may be found in [22, 23].

Since the beginning of its science operation, PFS has been collecting Martian atmospheric spectra, currently covering more than 7 Martian years (MY 26 to MY 34). In this work, we have selected only several PFS nadir spectra representative of different Martian conditions, especially in terms of seasonal and latitudinal variations of CO (see section 5.1 for details). Among the two channels, only the SWC spectral range covers the vibrational bands of CO (the 1-0 at 2143 cm^{-1} and the 2-0 at 4235 cm^{-1}). This work has only used apodized SWC spectra in the region of the much stronger 1-0 band of CO.

3. Radiative transfer

The monochromatic infrared radiance at wavenumber $\tilde{\nu}$ measured by PFS at the top of the Martian atmosphere (TOA), $I^{\uparrow}(\tilde{\nu}, \theta, \mathrm{TOA})$, can be described by the sum of two terms: 1) the transmission of the radiance emitted and

reflected by the Martian surface, and 2) the contribution of scattering and emission by the atmosphere. This is expressed by the equation of the radiative transfer:

$$\begin{aligned} I^{\uparrow}(\tilde{\nu},\theta,\mathrm{TOA}) &= I^{\uparrow}(\tilde{\nu},\theta,0)\,t(\tilde{\nu},\theta,0,\mathrm{TOA}) \\ &\quad + \int_0^{\mathrm{TOA}} J(\tilde{\nu},\mathbf{\Omega},z)\,\frac{\partial t(\tilde{\nu},\theta,z,\mathrm{TOA})}{\partial z}\,\mathrm{d}z\,, \end{aligned} \tag{1}$$

where θ is the ground zenith angle, $t(\tilde{\nu},\theta,0,z)$ is the transmittance of the Martian atmosphere, $t(\tilde{\nu},\theta,z,\mathrm{TOA})$ is the transmittance between altitude z and TOA, $J(\tilde{\nu},\mathbf{\Omega},z)$ is the atmospheric source term which depends on thermal emission and scattering and where $\mathbf{\Omega}$ represents the geometric angles. Note that in this work, only clear or almost clear atmospheres (see section 5.1) have been analysed. In this case, scattering can be neglected and the atmospheric source function can be approximated by a Plank function $B(\tilde{\nu},T)$. The radiance at the surface, $I^{\uparrow}(\tilde{\nu},\theta,0)$, takes into account the emission of the ground and the reflection of the solar incoming radiation as follow:

$$I^{\uparrow}(\tilde{\nu},\theta,0)) = \epsilon(\tilde{\nu})B(T_s) + (1-\epsilon(\tilde{\nu}))I_0^{\downarrow\dagger}(\tilde{\nu}) + r(\tilde{\nu},\theta,\phi,\theta^{\star},\phi^{\star})F_0^{\downarrow\star}(\tilde{\nu}), \tag{2}$$

where $B(T_s)$ is the Planck function at surface temperature T_s, $\epsilon(\tilde{\nu})$ is the wavenumber dependent emissivity of the Martian surface, $I_0^{\downarrow\dagger}$ is the mean radiance associated to the downward flux of the atmosphere and $F_0^{\downarrow\star}(\tilde{\nu})$ is the solar flux reaching Mars' surface. $r(\tilde{\nu},\theta,\phi,\theta^{\star},\phi^{\star})$ is the effective reflectivity of the surface. $\theta^{\star}$ and $\phi^{\star}$ are respectively the zenithal and azimuthal angles of the Sun, and ϕ is the azimuthal angle of the satellite.

In order to calculate the TOA radiance, equation 1 is discretized into a set of layers, in which, the averaged temperature, pressure, and partial columns of molecular species are calculated. The upwelling radiance at the top of layer i is estimated as

$$I_i^{\uparrow} = B(\overline{T}_i) + (I_{i-1}^{\uparrow} - B(\overline{T}_i))\tilde{t}_i, \tag{3}$$

where $B(\overline{T}_i)$ is the emission of layer i approximated as a blackbody at the averaged temperature $\overline{T}_i$. The effective transmittance $\tilde{t}_i$ of layer i is calculated using

$$\tilde{t}_i = \exp\left[-\sum_j PC_{i,j}\sum_{j,k}\sigma_{j,k}(\tilde{\nu},\overline{P}_i,\overline{T}_i)\right], \tag{4}$$

where j is associated to the molecular species and k to the relevant absorption lines at the chosen $\tilde{\nu}$. $PC_{i,j}$ is the partial column of species j in layer i and $\sigma_{j,k}(\tilde{\nu}, \overline{P}_i, \overline{T}_i)$ is the absorption cross section of that species (cm^2/molecules) calculated for the mean parameters of layer i.

In this work, the Atmosphit software has been used for radiative transfer calculations. It is a versatile line-by-line radiative transfer code initially developed for Earth atmosphere, but which can easily be adpated for Mars. Details about the Atmosphit software can be found in [24], [25] and [26]. For this work, the emissivity and the effective reflectivity introduced in equation 2 are considered constant with wavenumber, and for the latter, a combined contribution of lambertian and specular reflections of the Sun radiation is assumed.

4. Retrieval method: Optimal estimation

4.1. Background

The method used in this work to retrieve the vertical profiles of CO is the optimal estimation [20]. The idea of this method is to find the CO profile that is the most consistent with both PFS observations and a certain prior knowledge of its distribution in the Martian atmosphere. This is done by minimizing the following cost function ϕ

$$\phi = (\mathbf{y} - \mathrm{F}(\mathbf{x}, \mathbf{b}))^{\mathrm{T}} {\mathbf{S}_{\boldsymbol{\epsilon}}}^{-1} (\mathbf{y} - \mathrm{F}(\mathbf{x}, \mathbf{b})) + (\mathbf{x} - \mathbf{x_a})^{\mathrm{T}} {\mathbf{S_a}}^{-1} (\mathbf{x} - \mathbf{x_a}), \quad (5)$$

where $\mathbf{y}$ is the measurement vector, consisting of the PFS spectral radiances, $\mathbf{x}$ is the atmospheric state vector, containing the variables to be retrieved, i.e. the CO profile but also the other parameters (see section 5.3), $\mathbf{b}$ includes all the other fixed atmospheric variables that influence PFS measurements, $\mathbf{x_a}$ is the *a priori* CO profile and F is the forward radiative transfer model. The covariance matrices, $\mathbf{S}_{\boldsymbol{\epsilon}}$ and $\mathbf{S_a}$, are respectively the measurement and the *a priori* covariance matrices.

The minimization of ϕ is iteratively performed by the Atmosphit software using the numerical Gauss-Newton method for moderately non-linear cases [20]. At each iteration, a new state vector is evaluated using

$$\mathbf{x}_{i+1} = \mathbf{x_a} + (\mathbf{K}_i^{\mathrm{T}} {\mathbf{S}_{\boldsymbol{\epsilon}}}^{-1} \mathbf{K}_i + {\mathbf{S_a}}^{-1})^{-1} \mathbf{K}_i^{\mathrm{T}} {\mathbf{S}_{\boldsymbol{\epsilon}}}^{-1} \left[\mathbf{y} - \mathrm{F}(\mathbf{x}_i, \mathbf{b}) + \mathbf{K}_i(\mathbf{x}_i - \mathbf{x_a})\right], \quad (6)$$

where $\mathbf{K}$ is the Jacobian matrix, whose rows correspond to the derivatives of the TOA radiance with respect to the retrieved variables. The convergence

is reached when the absolute difference between the forward models of the two last iterations is lower than 20%. Note that Atmosphit does not retrieve the partial column in each layer directly but instead a scaling factor for each layer, which is applied to the *a priori* profile at the end of each iteration.

4.2. Characterization of the retrievals

4.2.1. Vertical sensitivity

The OEM offers a very adequate framework to characterize the retrieved CO profiles in terms of vertical sensitivity. This is done in this work mostly in terms of the averaging kernel matrix $\mathbf{A}$. It is defined as the sensitivity of the retrieved state (hereafter symbolized by $\hat{\mathbf{x}}$) to the true state ($\mathbf{x}$) and can be calculated as

$$\mathbf{A} = \frac{\partial \hat{\mathbf{x}}}{\partial \mathbf{x}} = (\mathbf{K}^{\mathrm{T}}{\mathbf{S}_{\boldsymbol{\epsilon}}}^{-1}\mathbf{K} + {\mathbf{S}_{\mathbf{a}}}^{-1})^{-1}\mathbf{K}^{\mathrm{T}}{\mathbf{S}_{\boldsymbol{\epsilon}}}^{-1}\mathbf{K}. \tag{7}$$

The rows of $\mathbf{A}$ define an averaging kernel function (AVK) for each element of $\hat{\mathbf{x}}$, which peaks at the altitude from where most of the information is coming. In other words, the AVK provide an estimation of the vertical sensitivity of the retrieval and peak at the altitude of maximum sensitivity. The trace of the $\mathbf{A}$ matrix gives the degrees of freedom for signal (DOFS), defined as the number of independent pieces of information in the retrieved profile.

4.2.2. Error analysis

As for the vertical sensitivity, a complete error budget analyses can be performed with the OEM, by separating different sources of errors from the total [20]. The following sources of errors have been evaluated:

1. The smoothing error: due to the limited vertical resolution of nadir observations, the retrieved state is a smoothed estimate of the true state. The resulting "error" can be characterized by the covariance matrix $\mathbf{S_s}$, calculated from the $\mathbf{A}$ and $\mathbf{S_a}$ matrices as follow

$$\mathbf{S_s} = (\mathbf{A} - \mathbf{I})\mathbf{S_a}(\mathbf{A} - \mathbf{I})^{\mathrm{T}}. \tag{8}$$

2. The measurement error, which directly propagates from the instrumental noise. Its associated covariance matrix can be written as:

$$\mathbf{S_m} = \mathbf{G}\mathbf{S}_{\boldsymbol{\epsilon}}\mathbf{G}^{\mathrm{T}}, \tag{9}$$

where $\mathbf{G}$ is the gain matrix, whose rows are the derivatives of the retrieved state with respect to the measurement. Note that in this work, forward modelling errors are included in the $\mathbf{S_\epsilon}$ matrix (see section 5.3). The covariance matrix $\mathbf{S_m}$ therefore describes the total error from the measurement noise and the forward model.

3. The error from the fitted parameters: this type of error comes from the correlations existing between the retrieved CO profile and the other retrieved parameters, such as the surface temperature (see section 5.3). Its covariance matrix is estimated using the non-diagonal elements $\mathbf{A_{nd}}$ of the AVK matrix:

$$\mathbf{S_f} = \mathbf{A_{nd}} \mathbf{S_a} \mathbf{A_{nd}}^{\mathrm{T}}. \tag{10}$$

The sum of the covariance matrices associated to these different uncertainties provide an estimation of the total retrieval error covariance matrix:

$$\mathbf{S_T} = \mathbf{S_s} + \mathbf{S_m} + \mathbf{S_f}. \tag{11}$$

The square root of the diagonal elements of $\mathbf{S_T}$ can be seen as the error on the retrieved CO at each altitude.

5. Spectra selection and retrieval set-up

5.1. Selection of spectra

CO vertical profiles have been retrieved from a small set of single nadir PFS observations. These observations have been chosen among all PFS measurements recorded between 10 January 2004 (MY 26) and 18 June 2017 (MY 34), following a 2 step procedure. The first step consists in finding spectra with almost clear sky conditions and sufficient signal-to-noise ratio (SNR) to detect CO lines in the 1–0 band. For this, only PFS observations associated to dust and ice column-integrated optical depths (τ_d et τ_i) lower than 0.15 have been considered (these two parameters were provided as part of the PFS L2 product by the National Institute of Astrophysics INAF-IAPS [15, 27]). Then, to guarantee sufficient SNR, only spectra meeting the following three criteria were kept:

- The radiance value at 2165.7 cm^{-1} has to be larger than 3 times the value of the noise, which was estimated to be 0.025 $\mathrm{erg\,s^{-1}\,sr^{-1}\,cm^{-2}\,cm}$ based on the standard deviation at 2165 cm^{-1} of several PFS spectra. This first criterion proves useful to discard PFS spectra with low radiance, but does not inform on the strength of CO absorption.

- The strength of the CO line at 2165.7 cm^{-1}, calculated in the brightness temperature (BT) space, has to be larger than 2.2 K (the noise equivalent temperature difference is estimated to be 1.1 K at 280 K). This strength is calculated as the difference (ΔBT) between the BT at 2165.7 cm^{-1} and the average brightness temperature of two channels chosen for the baseline (2163.6 cm^{-1} and 2167.8 cm^{-1}).

- The surface temperature (from the PFS L2 product) has to be larger than 240 K to remove spectra with very low surface contribution.

In total, 168793 spectra have passed this prefiltering procedure. Interestingly, all correspond to daytime observations.

After this first step, the selected PFS observations have been sorted in 5 latitude bands for the 4 seasons, as: the North Pole (60° to 90°), the mid-latitudes of the Northern hemisphere (30° to 60°), the Equator (−30° to 30°), the mid-latitudes of the Southern hemisphere (−60° to −30°) and the South Pole (−90° to −60°). The seasons are defined according to the solar longitude (LS): Northern spring/Southern Autumn (0° − 90°), Northern summer/Southern winter (90° − 180°), Northern autumn/Southern spring (180° − 270°) and Northern winter/Southern summer (270° − 360°). For each latitude band and each season, only one spectrum has been selected whenever possible. This has not been the case for the autumn and winter at both poles, characterized by very low source signals, especially during the polar night. The 16 selected spectra for this prospective study are listed in Table 1 and shown in Figure 1. Most of the them present a similar radiance of around 0.6–1.0 erg s^{-1} sr^{-1} cm^{-2} cm in the CO band; the three with the larger radiances (yellow curves except for the mid-latitudes of the Northern hemisphere) are associated to scenes with high surface temperature. All 16 spectra show very clear CO lines as expected and have corresponding dust and ice integrated opacities significantly smaller than 0.15.

Table 1: Selected PFS spectra. I_{2165} stands for the value at the radiance at 2165.7 cm^{-1}. ΔBT is the brightness temperature difference between a CO sensitive channel at 2165.7 cm^{-1} and two baseline channels (see text for details); τ_d et τ_i are the dust and ice integrated opacities; LS is the solar longitude and T_s is the surface temperature.

Latitude (°)	**Longitude** (°)	**LS** (°)	**T_s** **(K)**	**ΔBT** **(K)**	I_{2165} **(erg s^{-1} sr^{-1} cm^{-2} cm)**	τ_d	τ_i
-1.92	58.51	132.65	258.975	3.286	0.7896	0.043	0.021
-40.05	-119.41	2.12	256.248	3.475	0.7487	0.023	0.056
42.09	31.16	135.72	257.439	3.290	0.6055	0.003	0.063
-5.69	132.43	209.13	270.785	3.348	1.4084	0.066	0.014
-47.88	151.47	212.85	263.508	2.538	0.9339	0.125	0.006
-35.69	-155.81	155.82	248.405	2.316	0.5300	0.026	0.064
31.62	8.12	181.22	252.257	4.427	0.7496	0.067	0.024
-62.63	-134.47	262.90	274.909	2.360	1.4033	0.129	0.009
2.61	92.32	324.27	252.931	3.499	0.7845	0.044	0.011
30.09	-86.76	330.24	245.006	3.163	0.5609	0.033	0.054
-45.38	118.75	334.42	252.829	3.599	0.7657	0.081	0.049
52.81	-40.13	59.66	254.308	3.693	0.6115	0.067	0.013
-6.72	-5.32	65.89	256.132	3.612	0.6425	0.055	0.096
63.56	53.35	68.07	250.989	3.003	0.5484	0.091	0.052
72.81	53.45	104.70	244.707	3.223	0.5028	0.055	0.026
-76.37	26.78	305.11	252.301	3.771	0.8316	0.034	0.019

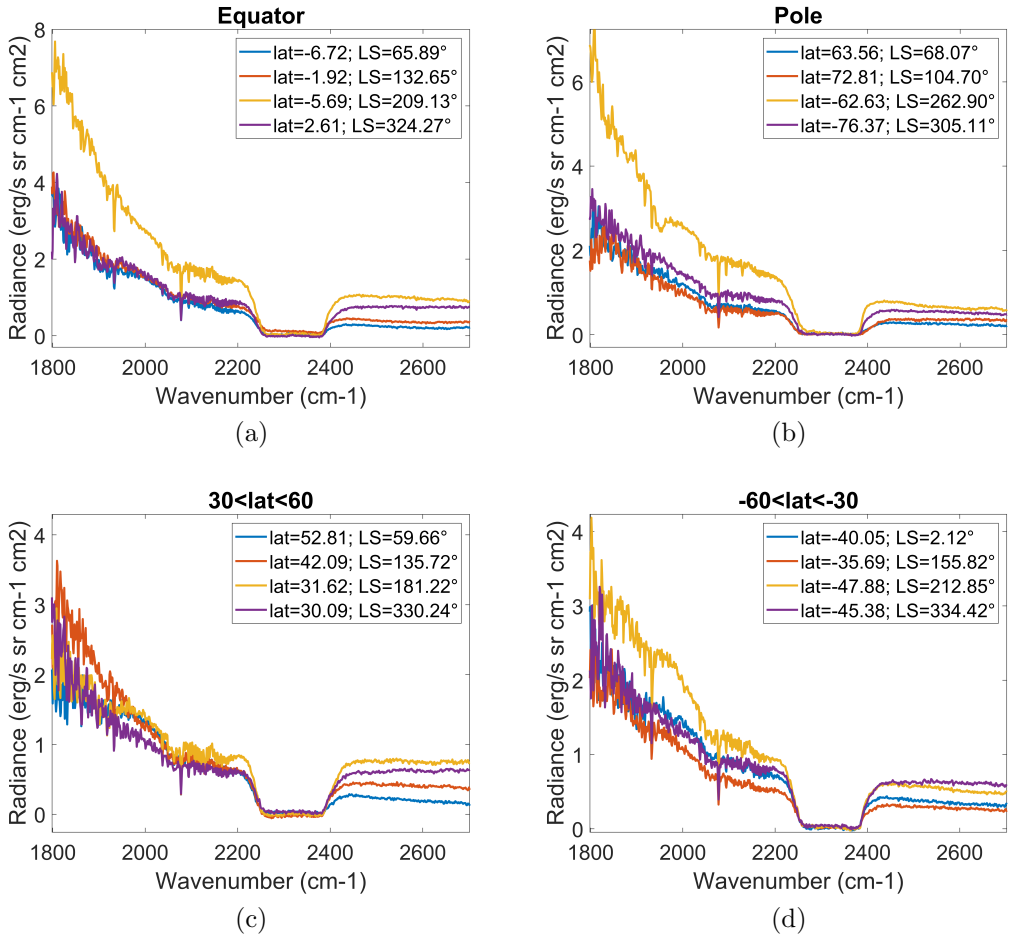


Figure 1: Selected spectra for each band of latitude; see also Table 1. Panel (b) shows the spectra selected for both North and South poles.

5.2. Input to radiative transfer

The radiative transfer equation has been solved for an atmosphere extending from 0 km to 60 km. For each single PFS spectrum, the temperature profile is fixed to the one retrieved independently by INAF-IAPS (see [27] for details). In the spectral range of the 1-0 band of CO, weak lines for the vibrational band ν_2 of water vapour (H_2O) and $\nu_1 + \nu_3$ of ozone (O_3) are possibly interfering and have been taken into account when simulating PFS observations. An averaged vertical profile has been considered for these two species and it has been kept fixed during the retrieval. The most adequate

value of surface emissivity has also to be considered, as errors on this parameter will propagate on the retrieved values of surface temperature and effective reflectivity, and hence ultimately on the retrieved CO vertical profile. The Planetary SUrface Portal [28, 29] provides global maps of the emissivity of the surface at 5 μm (2000 cm^{-1}) on spatial grids of $0.025^\circ \times 0.025^\circ$ resolution; they were built from OMEGA/MEX observations taken over 3 Martian years (MY 27-30) [30]. The emissivity values for the grid box corresponding to the selected PFS spectra have been considered in the retrieval. The spectroscopic parameters have been taken from HITRAN 2016 [31], including the pressure broadening due to CO_2.

The PFS spectra analysed in this work are apodized by an Hamming function. Several instrumental effects (due to e.g. misalignments) are, however, such that the instrumental line shape (ILS) has a FWHM of around 1.8 cm^{-1} and differs slightly from the theoretical Hamming function. We have tested two different formulations of the ILS, which ultimately were shown to give very similar quality of fits. An example of the residuals (observed–calculated) obtained after fitting is shown in Figure 2. The first corresponds to the ILS formulation provided by INAF-IAPS and which is the recommended one for the community; it leads to the best fit for half of the 16 spectra. The second one (hereafter called "HG") stems from the theoretical Hamming function, but slightly modified with an off-axis angle (misalignment in the interferometer), to introduce a small asymmetry in the function [32], and with second-order auto-apodization effects. This second one leads to the best fits for the other half of the 16 spectra analysed in this work. For consistency with previous works, all results presented in the following are those obtained using the ILS provided by INAF-IASP. The comparison between the two sets of fits is used later on section 6.2.3 to discuss the error possibly introduced by an imperfect ILS.

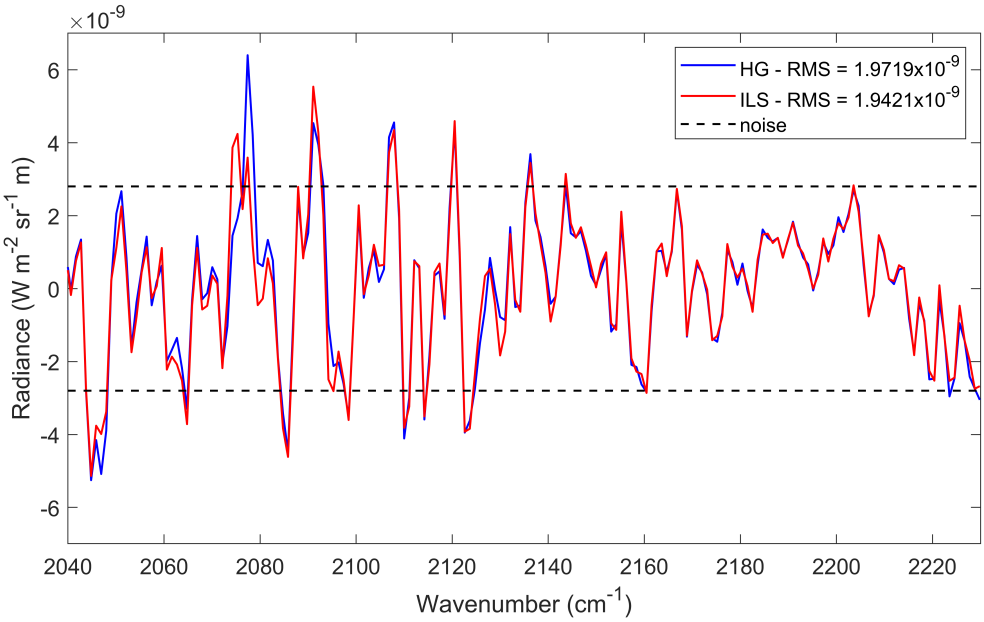


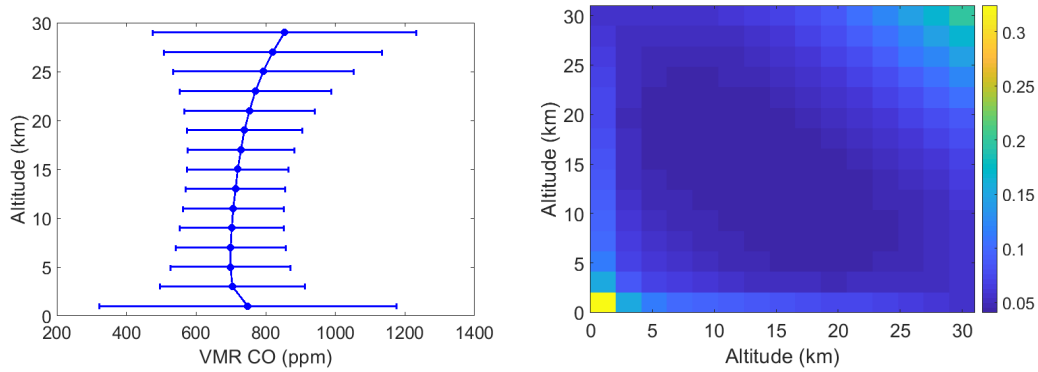
Figure 2: Example of residuals between the observed and fitted spectra calculated for the case using the HG function (blue) and the ILS provided by the INAF-IAPS (red). The RMS are shown for each case.

5.3. Retrievals settings

The retrieval of CO vertical profiles has been performed in two steps. In the first step, a large spectral range from 2040 to 2600 cm^{-1} was adjusted with the objective to obtain an accurate value for the effective surface reflectivity, which can then be used in the second step. The *a priori* value of the reflectivity has been set to 0.023 and its associated variability to 20%. The retrieved reflectivity is fed into the second and main step, which consists in the retrieval of the vertical profile of CO. It is performed on a shorter spectral range, going from 2040 to 2230 cm^{-1}. Specifically, the CO vertical profiles are retrieved for 2 km thick layers from 0 to 24 km. The *a priori* profile $\mathbf{x_a}$ and covariance matrix $\mathbf{S_a}$ used to constrain the CO retrieval have been built from a global ensemble of modelled profiles from the Mars Climate Database (MCD, version 5.3) [7, 33] for one Martian year (climatology solar average scenario). These profiles were simulated on a spatial grid of 3.75° × 5.625° (latitude × longitude) for one day per Martian month (defined as a period of 30° LS). This day corresponds to the centered LS of the month and CO profiles were calculated every 2 Martian hours (1 Martian hour is defined as

$1/24^{th}$ of a sol). In total, 451584 CO profiles have been considered. The resulting $\mathbf{x_a}$ profile and the $\mathbf{S_a}$ matrix are shown in Figure 3 for the 2 km thick layers that have been retrieved over the altitude range from 0 to 24 km. The *a priori* profile shows an almost uniform vertical distribution of CO at a volume mixing ratio (VMR) of about 700 ppm between 5 and 15 km. Close to the surface, the VMR increases to about 750 ppm and from 15 km of height, it starts to increase slightly due to the photodissociation of CO_2 at higher altitudes. The largest *a priori* variability is at the surface, where it reaches 57%. It then decreases with altitude and drops to a minimum of 20% in the 12–14 km layer. From this minimum, the *a priori* variability starts to increase again. Also noteworthy and of high relevance for this work is that the $\mathbf{S_a}$ presents non-negligible correlation between the different layers, meaning that the value of the profile retrieved at one given altitude will be influenced significantly from layers above and below. On a minor point, note that the $\mathbf{S_a}$ originally built from the model had unphysical correlation between the surface layer and the very high atmosphere, which were removed.

In the main step of the retrieval, in addition to the CO profile, the surface temperature and the profile of CO_2 have been retrieved simultaneously, which allows recalculating more accurately the CO VMR at the last iteration. The *a priori* uncertainty of the surface temperature has been set to 20%. The *a priori* vertical profile of CO_2 and its associated variability have been determined using the model output, in the same way as for CO (see above). The CO_2 *a priori* profile is almost uniform, with a mole fraction of around 0.963, and the prior uncertainty is very small, largest close to the surface (2.2%) and then around 0.5% at higher altitudes. Despite the low variability allowed on the CO_2 profile, fitting the latter slightly improved the quality of the fits in most cases. Finally, the $\mathbf{S_\epsilon}$ has been considered diagonal with a value for $\boldsymbol{\sigma_\epsilon}$ of 0.028 erg s^{-1} sr^{-1} cm^{-2} cm, larger than the one discussed in section 5.1 to take into account forward modelling errors.



(a) (b)

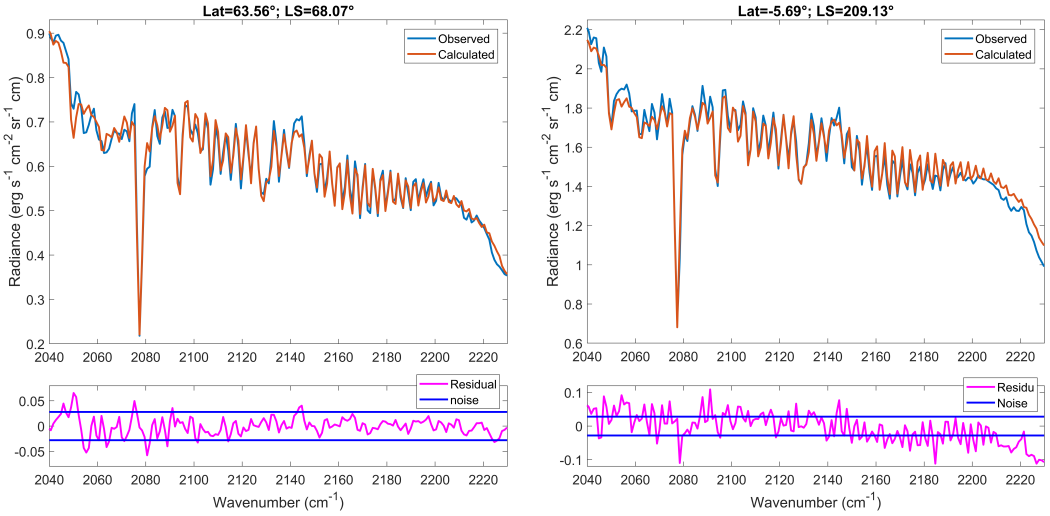
Figure 3: A priori profile (left) and covariance matrix (right) built using a representative ensemble of CO profiles from the MCD database (climatology solar average scenario). The matrix is expressed in multiplicative factor. The error bars on the profile correspond to the square root of the diagonal elements of the matrix, applied on the VMR.

6. Results

6.1. Spectral fittings and retrieved profiles

With this choice of retrieval parameters, the 16 spectra are fitted well, with the RMS of the residual varying between 1.9×10^{-2} erg s^{-1} sr^{-1} cm^{-2} cm and 4.6×10^{-2} erg s^{-1} sr^{-1} cm^{-2} cm. Among all spectra, 9 have a RMS lower than the level of $\boldsymbol{\sigma_\epsilon}$ considered (2.8×10^{-2} erg s^{-1} sr^{-1} cm^{-2} cm). Figure 4 illustrates the quality of the fits for the two extreme cases, with respectively the lowest (Figure 4.a) and largest RMS (Figure 4.b) obtained. For the lowest RMS case, the residual of the fit lays well within the level of $\pm\ \boldsymbol{\sigma_\epsilon}$ we have considered. For the highest RMS case, some spectral features remain above the noise level. This is the case in the R branch of the CO band, where the fitted spectrum is too high in radiance, mainly due to the difficulty of reproducing accurately the baseline of the spectrum, which is affected by the surface emissivity, reflectivity and temperature but also the CO_2 continuum. It is worth noting that the surface radiance is significantly higher in this case (around 2 erg s^{-1} sr^{-1} cm^{-2} cm at 2050 cm^{-1}, almost twice larger) than for the lowest RMS case. The increase of the RMS with the radiance level seems to be a general behaviour among the 16 spectra analysed. Overall, we find that the average RMS is very similar to the $\pm\ \boldsymbol{\sigma_\epsilon}$

value considered in $\mathbf{S}_{\boldsymbol{\epsilon}}$, suggesting that the choice is appropriate and in some cases quite conservative.



(a) (b)

Figure 4: Example fits among the 16 PFS spectra analysed. For the case (a) with the lowest RMS of the residual (1.9×10^{-2} erg s^{-1} sr^{-1} cm^{-2} cm) and, (b) the largest RMS (4.6×10^{-2} erg s^{-1} sr^{-1} cm^{-2} cm).

Figure 5 shows the retrieved CO profiles for three representative cases. Above 5 km of height, all retrieved profiles present a similar shape as the *a priori* profile, although not exactly at the same VMR. In the last layer, the maximal difference between the retrieved CO VMRs is equal to 457 ppm, with a minimum and a maximum CO VMRs respectively of 514 and 971 ppm. Closer to the Martian surface, the variability in the retrieved CO VMRs around the *a priori* is larger, with a minimum and a maximum of respectively 313 ppm (spectrum recorded in the South Pole during Southern spring) and 1687 ppm (spectrum recorded in mid-latitudes of the Northern hemisphere during Northern autumn), leading to a maximal difference of 1374 ppm. This departure from the *a priori* tends to show that the sensitivity of PFS observations is significant close to the surface, and this will be discussed in more details in the next section. The column averaged CO VMR varies from 464 ppm to 1115 ppm, and is in good agreement with previous measurements of CO in the Mars atmosphere (see section 6.3). These values are associated

with total columns of CO falling within 8.83×10^{19} molecules/cm^2 and 2.76×10^{20} molecules/cm^2.

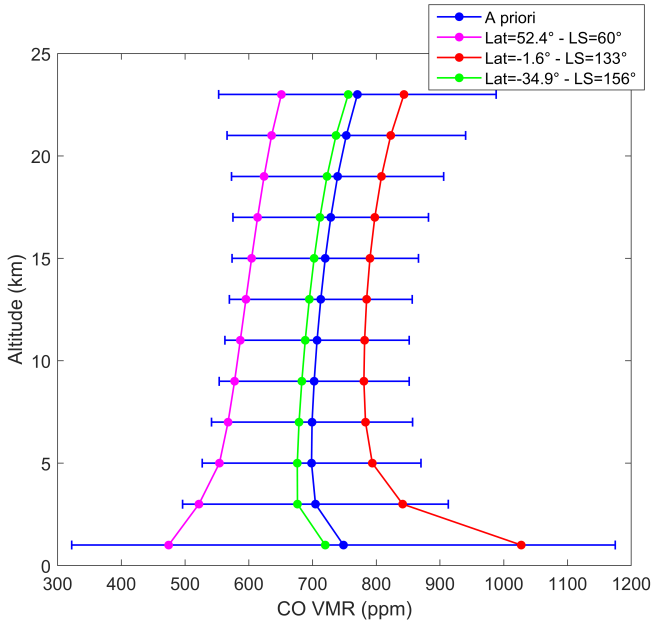


Figure 5: Examples of retrieved CO profiles. The VMRs correspond to the averaged VMRs of each retrieved layer (every 2 km). The *a priori* profile is shown in blue along with the associated *a priori* variability (square root of the diagonal element of the $\mathbf{S_a}$).

6.2. Characterization of the retrieved profiles

6.2.1. Vertical sensitivity

The vertical sensitivity of the retrieval can be firstly described with the Jacobians, which provide an estimation of the sensitivity of the TOA radiance to a change of the CO concentration in a certain layer. The Jacobians for one out of the 16 spectra is shown as an example in Figure 6 (note that they are similar for all spectra). As seen from Figure 6, for the entire spectral range, the Jacobians reach their largest value close to the surface, showing that this is where the nadir PFS observations have the maximal sensitivity to CO. The values of the Jacobians then decrease with altitude to finally 0 above 15 km, where the sensitivity of PFS measurements to CO is vanishing. An important results that follows is that the sensitivity is altitude dependent and that this *a posteriori* justifies the idea of fitting a profile rather than a column. It is also worth pointing that the PFS sensitivity to CO is not

constant over the whole spectral range used for the retrieval: the instrument is more sensitive to CO in the strongest R2 to R8 lines (2154–2176 cm^{-1}) for the R-branch and in the P3 to P8 lines (2111–2131 cm^{-1}) for the P-branch.

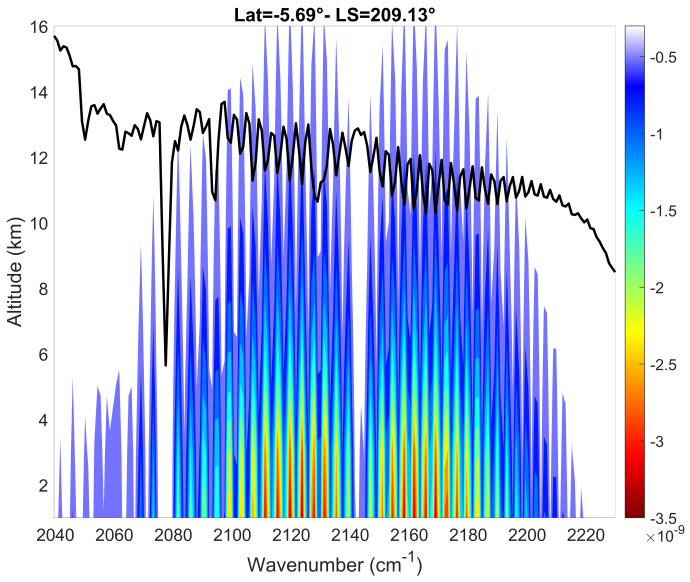
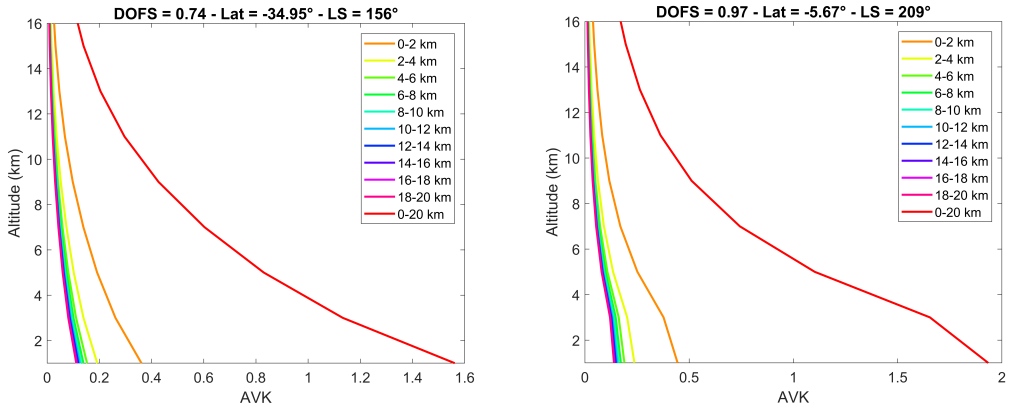


Figure 6: Example of Jacobians (W m^{-2} sr^{-1} m per scaling factor, color scale) calculated the PFS observation at -5.69 latitude and 132.43 longitude; 209.13 LS. The corresponding spectrum is shown in black.

The maximal sensitivity that PFS has to CO close to the surface is confirmed by the AVK functions, which are shown in Figure 7 for the lowest (a) and highest (b) DOFS cases. For all retrieved layers, the AVK functions peak at the surface, with values ranging between 0.36 and 0.44. The width of the AVK is large, with each function spanning the range from 0 to about 12 km. This shows that all retrieved layers are correlated with each other and especially that the information in the upper altitudes is mostly driven by the retrieval at the near-surface. While nadir TIR sounders on Earth have generally low sensitivity to the surface (e.g. IASI, [19]) this is obviously not the case here. There are two reasons for this: 1) the thermal contrast associated to the 16 selected observations varies between 15 K and 64 K, which is high, compared to the usual values encountered on Earth, and even more importantly 2) the contribution of the reflected solar radiation to the upwelling surface radiance is more significant in the case of Mars than for

Earth, which makes the dependency to thermal contrast less relevant. Note finally that above 15 km, all the AVK functions drop close to 0; the CO retrieval is no longer sensitive to the CO abundance in these layers.

The averaging kernels show that the retrieved profile is not resolved vertically. In fact among the 16 PFS observations, the DOFS varies between 0.74 and 0.97. This shows that the only quantity retrieved independently is the total column of CO. The variation of the DOFS is mostly related to that of the signal-to-noise ratio of PFS observations, and hence mainly to surface temperature and reflectivity. The dependence on thermal contrast is second-order and does not affect the values of the DOFS much. There is, however, a positive correlation between the first diagonal element of the AVK matrix (sensitivity of the retrieved CO column in the first layer to the true column in that layer) and the thermal contrast. On the contrary from the small set of spectra analysed, we did not observe a dependence of the vertical sensitivity on the abundance of CO.



(a) (b)

Figure 7: AVK functions associated to the retrieval of CO profile for the case with the lowest DOFS (a), and for the case with the highest DOFS (b). The DOFS is indicated on top along with latitude and solar longitude.

6.2.2. Error budget

The different sources of error on the retrieved CO profile have been evaluated from equations 8, 9, 10 and 11 along with the total error. Figure 8 shows the vertical distribution of these errors for two cases: the one with the lowest uncertainty (Figure 8.a) and the one with the highest uncertainty

(Figure 8.b). For all 16 spectra, the largest error is found at the surface (where the prior uncertainty is the largest), and varies between 26% and 32%. The retrieval error then decreases with height. Above 5 km, it stays almost constant and varies between 10% and 13%. Overall, at all altitudes, the prior uncertainty is reduced by around 50%, showing the improvement in the knowledge of the CO vertical distribution brought by PFS measurements. The total retrieval error on the total column of CO is between 5 and 15%, which is promising in the perspective to study the CO spatial and temporal variability on Mars.

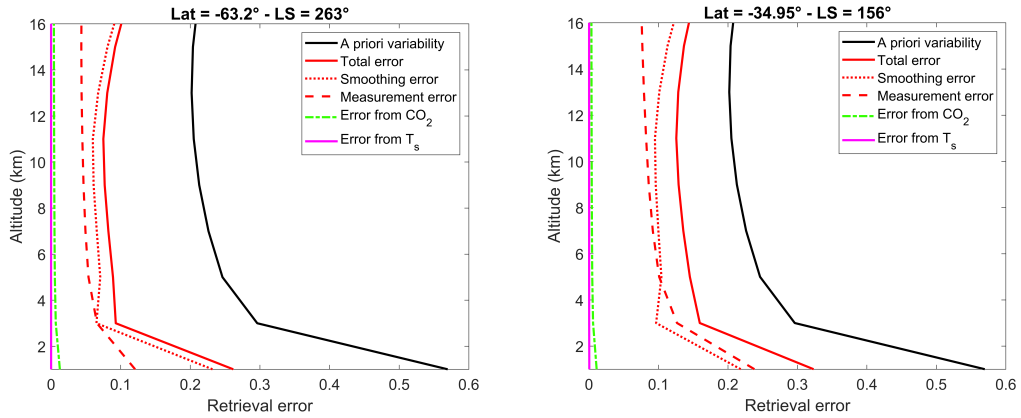


Figure 8: Vertical distribution of the total error on the retrieved CO profile and of the different sources of uncertainty. Two cases are shown: the one with the lowest total error (a) and the one with the highest error (b). The *a priori* variability is shown as the black line.

As seen from Figure 8, the two main sources of uncertainty are the smoothing and the measurement errors, which have very similar contributions to the total retrieval error. Above 6 km, the smoothing error is generally the largest and varies between 6% and 11%. The measurement error is lower in this altitude range and varies between 5 and 9%. At the surface, the measurement error varies between 12% and 24% depending on the strength of the radiance, and the smoothing error is around 23%. In Figure 8, we can see that the contributions of the uncertainties on the CO_2 profile and surface temperature are below 1%; this small impact is related to the fact that these two parameters are retrieved along with the CO profile.

6.2.3. Other factors affecting the retrievals

Here we discuss the impact on the profile retrievals and their characterization of two factors: the choice of the $\mathbf{S_a}$ matrix to constrain the profile, and that of the ILS formulation (see also discussion in section 5.2). In order to test the *a priori* covariance matrix, we have repeated the CO retrievals for four observations out of the 16, with an *ad hoc* matrix, showing 50% variability at all levels (i.e. the diagonal elements are all equal to 0.25) and a correlation length of 11 km (exponential decay from the diagonal elements). The results, presented in Figure 9 (a), clearly show spurious oscillations of the retrieved VMR as compared to the retrievals with the model-derived $\mathbf{S_a}$, Figure 9 (b). This is a simple but solid illustration of the need to consider realistic constrains in retrieving vertical profiles from nadir observations.

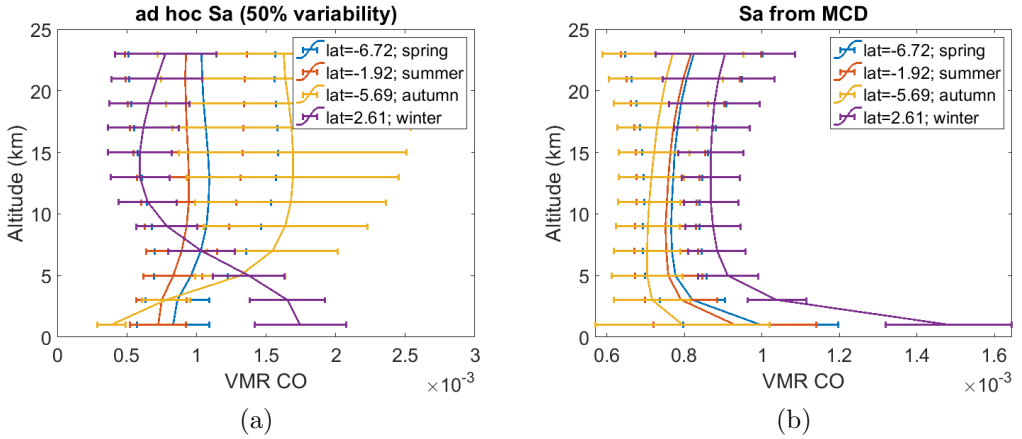


Figure 9: The retrieved CO profiles on the equator for different season by testing two *a priori* covariance matrices.

As mentioned in section 5.2, two different ILS have been found to give similar fits quality of PFS observations. The baseline chosen for this work is the one recommended by the PI team of PFS (hereafter called "PILS") and in this section, we evaluate the impact of this choice on the retrieved CO profile by also evaluating the results obtained with the modified Hamming function (HG). This is done by calculating, for each observation, the relative difference (RD) between the retrieved CO profiles using the two ILS modes as $RD = \frac{(CO_{PILS} - CO_{HG}) \times 100}{CO_{PILS}}$. The average relative difference for all the retrieved layers is shown in Figure 10. It is clear from this figure that the choice of

the ILS function has a small but non negligible effect on the retrieved CO profile. The CO VMR is systematically higher when using the PILS, with a maximum relative difference at the surface, where it reaches 9%. It then decreases to around 3% at higher altitudes. On the total column of CO, this translates to relative differences around 5% on average. It is useful to have these differences in mind for future work, as these can be taken as a systematic uncertainty on the retrieved CO profile and columns.

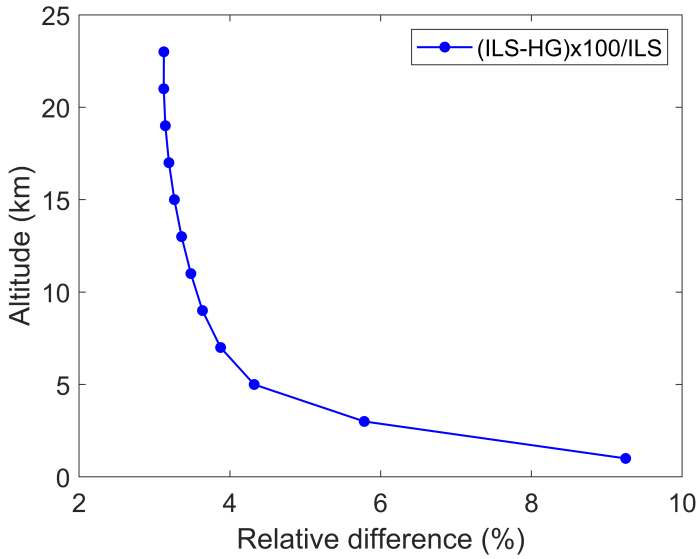


Figure 10: Average relative difference between the CO profiles retrieved with the ILS recommended by the PI team of PFS and the HG ILS adjusted in this work.

6.3. Comparison with previous measurements

Previous measurements have reported that the globally averaged CO VMR is around 800 ppm [17]. It has also been shown that CO presents strong latitudinal and seasonal variations, especially in the polar regions, where it is mainly due to variations of the CO_2 surface pressure related to its alterning condensation and sublimation. In autumn/winter, CO_2 condenses indeed on the polar ice cap, leading to a decrease of the CO_2 pressure and, as a result, to an increase of the CO VMR. The reverse happens during spring/summer, when the CO_2 ice sublimates. The retrieved CO profiles in this work are consistent with these processes. This is shown with Figure 11, where the retrieved column-average CO VMRs are shown as a function of

latitude and LS. The drop of the VMRs is well observed at both poles in summer, with averaged values around 650 ppm for the North Pole and 500 ppm for the South Pole. It is worth stressing again that we did not find PFS observations with detectable CO lines for the poles during the winter, so that the expected increase of the VMRs during this period cannot be confirmed. The averaged CO VMR retrieved in this work from the PFS observations located equatorward is around 830 ppm and in good agreement with the global average calculated in other studies [17].

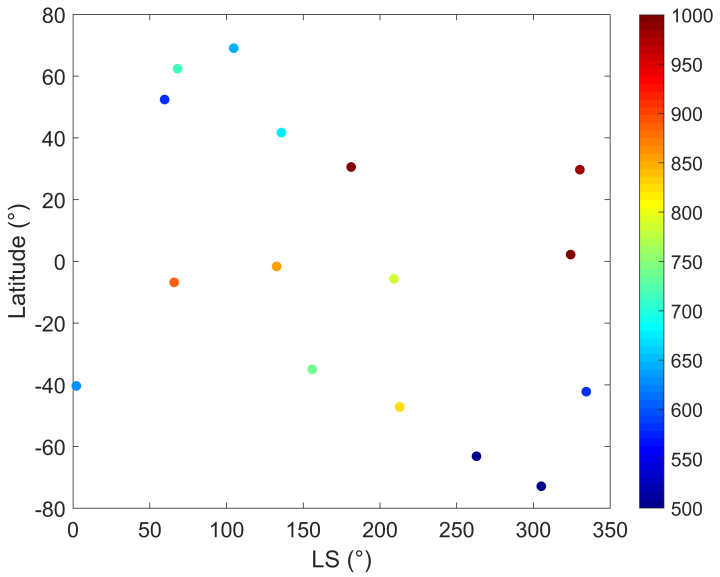


Figure 11: Column-averaged CO VMRs (color scale, ppm) calculated from the retrieved profiles as a function of latitude and LS. Note that the PFS observations correspond to different Martian years.

The column-averaged VMR calculated from the retrieved CO profiles are also in reasonable agreement with that reported in other studies. Table 2 compares the CO column-averaged VMRs from this work to 1) that retrieved from CRISM observations by [17] and 2) from PFS observations by [14]. The agreement is better with [17], with no obvious bias but differences that can reach around 200 ppm; these are most likely due to 1) longitudinal variations and 2) inter-annual variability. The mitigated comparison with [14], which at first sight is unexpected considering that they relate to the same instrument, is likely due to the fact that the two studies use different spectral bands to

retrieve CO: the 1–0 fundamental band for this work and the weaker 2–0 overtone around 4300 cm^{-1} in [14]. While the source radiance is obviously higher in the shortwave, the weakness of the CO absorption could result in larger retrieval errors. The limitation of using the fundamental band, as done here, is that it requires sufficient reflectivity and/or surface temperature. For this first study, only spectra with good signal-to-noise have been considered and this gives us strong confidence in the retrieved VMRs; this is reinforced by the good agreement with [17]. A better understanding of the source of the differences between our work and [14] would require more analyses on a larger set of spectra in a future work.

Table 2: Comparison of the CO column-averaged VMRs using the retrieved profiles of this work with values reported by [17] and [14]. More particularly, the comparison is made with the CO VMRs shown in Figure 3 of [17] and which span 5 Martian years (MY28–MY33). Regarding the work of [14], the comparison is made with CO VMRs reported in their Figure 10, which shows the latitudinal and seasonal variations of CO for 2.5 Martian years. The values/ranges indicated for [17] and [14] are therefore indicative and should not be taken as the exact values.

Latitude (°)	**Longitude (°)**	**LS (°)**	**CO VMRs (total column, ppm)**		
			This work	[17]	[14]
-1.92	58.51	132.65	856	850–900	500–520
-40.05	-119.41	2.12	632	750–800	2400
42.09	31.16	135.72	679	700	250–300
-5.69	132.43	209.13	788	1000	/
-47.88	151.47	212.85	822	650–700	/
-35.69	-155.81	155.82	738	1000–1050	200
31.62	8.12	181.22	1115	900	1100
-62.63	-134.47	262.90	464	400–450	/
2.61	92.32	324.27	1085	800–850	1100
30.09	-86.76	330.24	981	800–850	250–300
-45.38	118.75	334.42	584	800–850	2200
52.81	-40.13	59.66	580	600–650	700–800
-6.72	-5.32	65.89	885	800	1000–1100
63.56	53.35	68.07	719	500–550	300–400
72.81	53.45	104.70	647	600–650	200–250
-76.37	26.78	305.11	491	400	800–900

7. Conclusions

The retrieval of CO vertical profiles from nadir observations on Mars has been performed for the first time. This has been achieved on high-spectral resolution measurements made by the PFS instrument on Mars Express, in the region of the 1–0 fundamental band of CO. Despite the fact that only a very small set of spectra with sufficient signal-to-noise ratios has been considered in this exploratory study, our results have clearly demonstrated the potential of using this spectral range for monitoring CO spatially and temporally on single PFS observations, except in the polar winters. The CO profiles have been retrieved using the optimal estimation method, with *a priori* information (*a priori* profile and variance-covariance matrix) built from a large ensemble of global model profiles, which we have shown to provide appropriate constrains. The CO profiles retrieved are very weakly resolved vertically, with the PFS spectra carrying no more than one piece of information. The vertical sensitivity is, however, altitude-dependent (sensitivity from 0 to about 20 km, maximal at the surface) and this alone justifies the retrieval of the profile. The errors on each level of the profile vary between 25% close to the surface to less than 10% above 3 km, due to the combined contribution of the measurement noise and the smoothing error. This translates to an error on the retrieved column or the column-averaged VMR of 5 to 15% depending on the scene. Other sources of errors have been identified and we have characterized in particular the one introduced by the uncertainty on the PFS ILS. In all cases we found that the PFS measurements substantially reduce the prior uncertainty on the CO profile and the column, and, as a result, that the retrieved CO abundances allow capturing the spatial and seasonal variability of CO on Mars. We found general agreement, considering the different periods and places, with CO abundances retrieved from the CRISM spectrometer. The agreement with independent studies from PFS is worse and likely related to the use of different spectral bands in the retrievals (the first overtone in earlier work and the fundamental band in this study). Generally, the possibility of retrieving CO with good accuracy from PFS single observations in the 1–0 band is very promising and stimulates larger-scale retrievals, which would provide strong constrains on the cycle of carbon species in the lowest (below 15 km) Martian atmosphere.

8. Acknowledgements

This work is funded by the FNRS CRAMIC project under grant number T.0171.16. PFS is funded by the Italian Space Agency under grant 2018-2-HH.0. Sophie Bauduin is Chargée de Recherches with FRS-FNRS. The authors would like to thank the LMD for providing the access to the Mars Climate Database, needed to build the *a priori* vertical profile CO and the associated covariance matrix.

9. References

[1] L. D. Kaplan, J. Connes, and P. Connes, "Carbon monoxide in the Martian atmosphere," *The Astrophysical Journal*, vol. 157, pp. L187–L192, 1969.

[2] M. B. McElroy and T. M. Donahue, "Stability of the Martian Atmosphere," *Science*, vol. 177, pp. 986–988, Sept. 1972.

[3] T. D. Parkinson and D. M. Hunten, "Spectroscopy and Acronomy of O_2 on Mars.," *Journal of Atmospheric Sciences*, vol. 29, pp. 1380–1390, Oct. 1972.

[4] S. K. Atreya and Z. G. Gu, "Stability of the Martian atmosphere: Is heterogeneous catalysis essential?," *Journal of Geophysical Research*, vol. 99, pp. 13133–13145, June 1994.

[5] S. K. Atreya and Z. G. Gu, "Photochemistry and stability of the atmosphere of Mars," *Advances in Space Research*, vol. 16, Aug. 1995.

[6] H. Nair, M. Allen, A. D. Anbar, Y. L. Yung, and R. T. Clancy, "A photochemical model of the martian atmosphere," *Icarus*, vol. 111, pp. 124–150, Sept. 1994.

[7] F. Forget, F. Hourdin, R. Fournier, C. Hourdin, O. Talagrand, M. Collins, S. R. Lewis, P. L. Read, and J.-P. Huot, "Improved general circulation models of the Martian atmosphere from the surface to above 80 km," *Journal of Geophysical Research: Planets*, vol. 104, no. E10, pp. 24155–24175, 1999.

[8] L. Neary and F. Daerden, "The GEM-Mars general circulation model for Mars: Description and evaluation," *Icarus*, vol. 300, pp. 458–476, 2018.

[9] S. K. Atreya and J. E. Blamont, "Stability of the Martian atmosphere - Possible role of heterogeneous chemistry," *Geophysical Research Letters*, vol. 17, pp. 287–290, Mar. 1990.

[10] F. Lefèvre, J.-L. Bertaux, R. T. Clancy, T. Encrenaz, K. Fast, F. Forget, S. Lebonnois, F. Montmessin, and S. Perrier, "Heterogeneous chemistry in the atmosphere of Mars," *Nature*, vol. 454, pp. 971–975, Aug. 2008.

[11] V. A. Krasnopolsky, "Spectroscopic mapping of Mars CO mixing ratio: Detection of north-south asymmetry," *Journal of Geophysical Research (Planets)*, vol. 108, p. 5010, Feb. 2003.

[12] T. Encrenaz, T. Fouchet, R. Melchiorri, P. Drossart, B. Gondet, Y. Langevin, J.-P. Bibring, F. Forget, and B. Bézard, "Seasonal variations of the martian CO over Hellas as observed by OMEGA/Mars Express," *Astronomy & Astrophysics*, vol. 459, pp. 265–270, Nov. 2006.

[13] F. Billebaud, J. Brillet, E. Lellouch, T. Fouchet, T. Encrenaz, V. Cottini, N. Ignatiev, V. Formisano, M. Giuranna, A. Maturilli, and F. Forget, "Observations of CO in the atmosphere of Mars with PFS onboard Mars Express," *Planetary and Space Science*, vol. 57, pp. 1446–1457, Oct. 2009.

[14] G. Sindoni, V. Formisano, and A. Geminale, "Observations of water vapour and carbon monoxide in the Martian atmosphere with the SWC of PFS/MEX," *Planetary and Space Science*, vol. 59, no. 2-3, pp. 149–162, 2011.

[15] M. Giuranna, P. Wolkenberg, D. Grassi, A. Aronica, S. Aoki, D. Scaccabarozzi, B. Saggin, V. Formisano, and the PFS team, "New dataset of atmospheric parameters retrieved by PFS-MEx." Abstract Scientific Workshop: From Mars Express to ExoMars, 2018.

[16] M. D. Smith, M. J. Wolff, R. T. Clancy, and S. L. Murchie, "Compact Reconnaissance Imaging Spectrometer observations of water vapor and carbon monoxide," *Journal of Geophysical Research: Planets*, vol. 114, no. E2, 2009.

[17] M. D. Smith, F. Daerden, L. Neary, and A. Khayat, "The climatology of carbon monoxide and water vapor on Mars as observed by CRISM and modeled by the GEM-Mars general circulation model," *Icarus*, vol. 301, pp. 117–131, 2018.

[18] S. Robert, C. Camy-Peyret, F. Daerden, M. De Mazière, E. De Wachter, L. Neary, S. Vandenbussche, and A. Vandaele, "Two test-cases for synergistic detections in the Martian atmosphere: Carbon monoxide and methane," *Journal of Quantitative Spectroscopy and Radiative Transfer*, vol. 189, pp. 86–104, 2017.

[19] S. Bauduin, L. Clarisse, M. Theunissen, M. George, D. Hurtmans, C. Clerbaux, and P.-F. Coheur, "IASI's sensitivity to near-surface carbon monoxide (CO): Theoretical analyses and retrievals on test cases," *Journal of Quantitative Spectroscopy and Radiative Transfer*, vol. 189, pp. 428–440, 2017.

[20] C. D. Rodgers, *Inverse methods for atmospheric sounding: theory and practice*, vol. 2. World scientific, 2000.

[21] V. Formisano, F. Angrilli, G. Arnold, S. Atreya, G. Bianchini, D. Biondi, A. Blanco, M. Blecka, A. Coradini, L. Colangeli, *et al.*, "The planetary Fourier spectrometer (PFS) onboard the European Mars Express mission," *Planetary and Space Science*, vol. 53, no. 10, pp. 963–974, 2005.

[22] M. Giuranna, V. Formisano, D. Biondi, A. Ekonomov, S. Fonti, D. Grassi, H. Hirsch, I. Khatuntsev, N. Ignatiev, M. Michalska, *et al.*, "Calibration of the Planetary Fourier Spectrometer short wavelength channel," *Planetary and Space Science*, vol. 53, no. 10, pp. 975–991, 2005.

[23] M. Giuranna, V. Formisano, D. Biondi, A. Ekonomov, S. Fonti, D. Grassi, H. Hirsch, I. Khatuntsev, N. Ignatiev, M. Malgoska, *et al.*, "Calibration of the Planetary Fourier Spectrometer long wavelength channel," *Planetary and Space Science*, vol. 53, no. 10, pp. 993–1007, 2005.

[24] B. Barret, D. Hurtmans, M. R. Carleer, M. De Mazière, E. Mahieu, and P.-F. Coheur, "Line narrowing effect on the retrieval of HF and

HCl vertical profiles from ground-based FTIR measurements," *Journal of Quantitative Spectroscopy and Radiative Transfer*, vol. 95, no. 4, pp. 499–519, 2005.

[25] P.-F. Coheur, B. Barret, S. Turquety, D. Hurtmans, J. Hadji-Lazaro, and C. Clerbaux, "Retrieval and characterization of ozone vertical profiles from a thermal infrared nadir sounder," *Journal of Geophysical Research: Atmospheres*, vol. 110, no. D24, 2005.

[26] C. Clerbaux, P.-F. Coheur, D. Hurtmans, B. Barret, M. Carleer, R. Colin, K. Semeniuk, J. McConnell, C. Boone, and P. Bernath, "Carbon monoxide distribution from the ACE-FTS solar occultation measurements," *Geophysical research letters*, vol. 32, no. 16, 2005.

[27] P. Wolkenberg, M. Giuranna, D. Grassi, A. Aronica, S. Aoki, D. Scaccabarozzi, and B. Saggin, "Characterization of dust activity on Mars from MY27 to MY32 by PFS-MEX observations," *Icarus*, vol. 310, pp. 32–47, 2018.

[28] F. Poulet, C. Quantin-Nataf, H. Ballans, K. Dassas, J. Audouard, J. Carter, B. Gondet, L. Lozach, J.-C. Malapert, C. Marmo, *et al.*, "PSUP: A Planetary SUrface Portal," *Planetary and Space Science*, 2017.

[29] C. Quantin-Nataf, L. Lozac'h, P. Thollot, D. Loizeau, B. Bultel, J. Fernando, P. Allemand, F. Dubuffet, F. Poulet, A. Ody, *et al.*, "MarsSI: Martian surface data processing information system," *Planetary and Space Science*, vol. 150, pp. 157–170, 2018.

[30] J. Audouard, F. Poulet, M. Vincendon, J.-P. Bibring, F. Forget, Y. Langevin, and B. Gondet, "Mars surface thermal inertia and heterogeneities from OMEGA/MEX," *Icarus*, vol. 233, pp. 194–213, 2014.

[31] I. E. Gordon, L. S. Rothman, C. Hill, R. V. Kochanov, Y. Tan, P. F. Bernath, M. Birk, V. Boudon, A. Campargue, K. V. Chance, B. J. Drouin, J.-M. Flaud, R. R. Gamache, J. T. Hodges, D. Jacquemart, V. I. Perevalov, A. Perrin, K. P. Shine, M.-A. H. Smith, J. Tennyson, G. C. Toon, H. Tran, V. G. Tyuterev, A. Barbe, A. G. Császár, V. M. Devi, T. Furtenbacher, J. J. Harrison, J.-M. Hartmann, A. Jolly, T. J. Johnson, T. Karman, I. Kleiner, A. A. Kyuberis, J. Loos, O. M. Lyulin,

S. T. Massie, S. N. Mikhailenko, N. Moazzen-Ahmadi, H. S. P. Müller, O. V. Naumenko, A. V. Nikitin, O. L. Polyansky, M. Rey, M. Rotger, S. W. Sharpe, K. Sung, E. Starikova, S. A. Tashkun, J. V. Auwera, G. Wagner, J. Wilzewski, P. Wcisło, S. Yu, and E. J. Zak, "The HITRAN2016 molecular spectroscopic database," *Journal of Quantitative Spectroscopy and Radiative Transfer*, vol. 203, pp. 3–69, 2017.

[32] J. Kauppinen and P. Saarinen, "Line-shape distortions in misaligned cube corner interferometers," *Applied Optics*, vol. 31, pp. 69–74, 1992.

[33] E. Millour, F. Forget, A. Spiga, T. Navarro, J.-B. Madeleine, L. Montabone, A. Pottier, F. Lefèvre, F. Montmessin, J.-Y. Chaufray, *et al.*, "The Mars Climate Database (MCD version 5.2)," in *European Planetary Science Congress 2015*, vol. 10, pp. EPSC2015–438, EPSC, 2015.